

Content-Addressable Memory with a Content-Free Energy Function

Félix Benoist,¹ Luca Peliti,² and Pablo Sartori^{1,*}

¹*Gulbenkian Institute of Molecular Medicine, Oeiras, Portugal*

²*Santa Marinella Research Institute, I-00058, Santa Marinella, Italy*

Content-addressable memory, *i.e.* stored information that can be retrieved from content-based cues, is key to computation. Besides natural and artificial neural networks, physical learning systems have recently been shown to have remarkable ability in this domain. While classical neural network models encode memories as energy minima, biochemical systems have been shown to be able to process information based on purely kinetic principles. This opens the question of whether neural networks can also encode information kinetically. Here, we propose a minimal model for content-addressable memory in which the kinetics, and not the energy function, are used to encode patterns. We find that the performance of this kinetic encoding approach is comparable to that of classical energy-based encoding schemes. This highlights the fundamental significance of the kinetic stability of kinetic traps as an alternative to the thermodynamic stability of energy minima, offering new insights into the principles of computation in physical and synthetic systems.

Introduction. The ability to recover multiple memories from cues of their content is a fundamental computation performed by natural and artificial neural networks [1–3]. The physical modeling of such a computational ability was pioneered by J.J. Hopfield in his celebrated 1982 article [4]. Reference [4] introduced an energy-based model for content-addressable memory, in which memories are modeled as patterns of activation of a fully-connected network of binary units representing neurons. The patterns are encoded via a set of energetic couplings and correspond to minima in the energy landscape of the network. Provided low crosstalk between patterns, each pattern can be retrieved via asynchronous updates from a content cue through equilibrium relaxation [2, 5].

In recent years, the performance of Hopfield networks has been significantly improved [6], with modern versions showing promising results in machine learning [3, 7–9]. More realistic networks of spiking neurons are also the subject of intense research in the context of biological neural computation [1, 10, 11]. Besides neurons, Hopfield-like encoding schemes have been used in models of biological liquid mixtures [12], multi-component self-assembly [13–15] and regulatory networks [16].

Although there are many variants of Hopfield networks, the patterns are always encoded as minima of an energy landscape [Fig. 1A]. In contrast, we propose a fundamentally new encoding approach based on tuning the kinetics of the pathways leading to the patterns; see Fig. 1B. In this framework, each pattern becomes a kinetic trap, which can only be retrieved transiently. Therefore, patterns are not more stable than other states but are more kinetically accessible. Although such kinetic encoding has already been used to differentiate binding partners in copolymerization [17–19] and self-assembly processes [20], in molecular error correction [18, 21, 22], and in frenetic steering of random

walkers [23], it is so far absent from Hopfield neural networks. We anticipate that this kinetic approach results in a functional content-associative memory network with capacity comparable to traditional Hopfield networks, but some unique characteristics (*e.g.* glassy behavior [24, 25]).

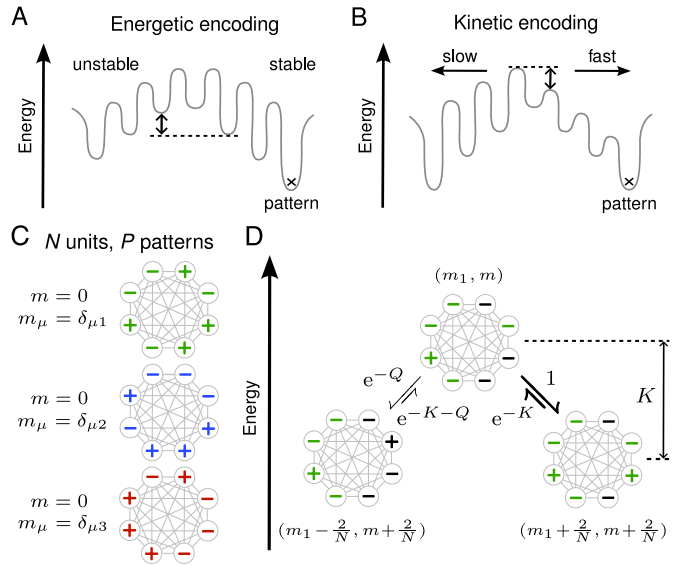


FIG. 1. *Schematics of kinetic encoding setup.* **A.** In energetic encoding, the pattern state is preferred due to its lower energy. **B.** In kinetic encoding, the pattern state is discriminated from other states with the same energy via the lower kinetic barriers along its pathway. **C.** $N = 8$ fully-connected units encode $P = 3$ activity patterns. The retrieval of pattern $\mu = 1$ corresponds to overlap values $(m_1, m_2, m_3) = (1, 0, 0)$ and activity $m = 0$. **D.** Sketch of the energy diagram for the retrieval of pattern $\mu = 1$ from a state with only -1 errors (black minus signs) besides the cue (green plus and minus signs). Going down in energy, the system can either create a $+1$ error (left transition) or correct a -1 error (right transition), the latter being kinetically favored.

* pablo.sartori@gimm.pt

Content-addressable memory. Consider N interacting binary units indexed $i = 1, \dots, N$, which represent neurons in a neural network. Each unit can be active or inactive, which we characterize by its activity value, $\sigma_i = +1$ or -1 , respectively. Among the 2^N system configurations, we select P different “pattern states” with activities denoted ξ_i^μ , where $\mu = 1, \dots, P$, see Fig. 1C. Hereafter, we assume that the patterns are random states with null mean. We quantify similarity between an arbitrary state and pattern μ through the overlap $m_\mu = \sum_i \sigma_i \xi_i^\mu / N$, which generalizes the activity $m = \sum_i \sigma_i / N$.

We consider a dynamics satisfying detailed balance, such that the transition rate from state $\boldsymbol{\sigma} = (\sigma_1, \dots, \sigma_i, \dots, \sigma_N)$ to $\boldsymbol{\sigma}' = (\sigma_1, \dots, -\sigma_i, \dots, \sigma_N)$ is given by

$$k(\boldsymbol{\sigma} \rightarrow \boldsymbol{\sigma}') = \frac{\omega(\boldsymbol{\sigma}, \boldsymbol{\sigma}')}{1 + \exp(\beta \Delta E(\boldsymbol{\sigma}, \boldsymbol{\sigma}'))}. \quad (1)$$

Here, β is the inverse temperature, $\omega(\boldsymbol{\sigma}, \boldsymbol{\sigma}') = \omega(\boldsymbol{\sigma}', \boldsymbol{\sigma})$ is a bare kinetic rate, and $\Delta E = \mathcal{H}(\boldsymbol{\sigma}') - \mathcal{H}(\boldsymbol{\sigma})$ is the energy difference, where \mathcal{H} is the system’s Hamiltonian. Note that the energy differences and the bare kinetic rates have different symmetries: Whereas $\omega(\boldsymbol{\sigma}', \boldsymbol{\sigma})$ is even in the exchange $\boldsymbol{\sigma} \leftrightarrow \boldsymbol{\sigma}'$, one has $\Delta E(\boldsymbol{\sigma}', \boldsymbol{\sigma}) = -\Delta E(\boldsymbol{\sigma}, \boldsymbol{\sigma}')$.

A model for content-addressable memory provides expressions for $\omega(\boldsymbol{\sigma}, \boldsymbol{\sigma}')$ and $\mathcal{H}(\boldsymbol{\sigma})$ that ensure pattern retrieval. That is, if the system is initialized with a cue for pattern $\mu = 1$, *i.e.*, in a state for which m_1 is small but non-zero and $m_{\mu \neq 1} \ll m_1$, then the system should evolve over time toward pattern 1: $\boldsymbol{\sigma} = (\xi_1^1, \dots, \xi_N^1)$. In this pattern state, $m_1 = 1$ and $m_{\mu \neq 1} \approx 0$, due to the near-orthogonality of patterns for large N [2].

Energetic encoding. In classical Hopfield networks, neurons are coupled via a matrix J_{ij} that encodes the P patterns [2, 4]:

$$J_{ij} = \frac{1}{N} \sum_{\mu=1}^P \xi_i^\mu \xi_j^\mu. \quad (2)$$

The Hamiltonian of the network is then defined as $\mathcal{H}(\boldsymbol{\sigma}) = -\frac{1}{2} \sum_{i,j \neq i} J_{ij} \sigma_i \sigma_j$. At low temperature, $\beta > 1$, this setup ensures pattern retrieval provided that $P < P_{\max}$, with $P_{\max} \sim N$ (see SI). Moreover, including higher-order couplings beyond the pairwise couplings of Eq. (2) leads to a dramatic increase in encoding capacity [26–28].

Crucially, this encoding is such that, for $P < P_{\max}$, the patterns are minima of \mathcal{H} . Since the original Hopfield network considered the limit $\beta \rightarrow \infty$, there was no discussion of bare kinetic rates. Later works at finite temperature [5, 29], as well as recent advances in energy-based models [9, 26, 28], all assume $\omega(\boldsymbol{\sigma}, \boldsymbol{\sigma}') = 1$, so that all information encoding is energetic, *i.e.* engraved in the Hamiltonian.

Kinetic encoding. We now provide an alternative approach to encoding patterns in Hopfield networks. We choose a Hamiltonian that is independent of the couplings J_{ij} defined in Eq. (2), but we let these couplings determine the bare kinetic parameters. Specifically, we set

$$\beta \mathcal{H}(\boldsymbol{\sigma}) = \frac{N}{2} K |m(\boldsymbol{\sigma})|, \quad (3)$$

where $K \geq 0$ is the energetic drive in units of β^{-1} . The $2^{N/2}$ states with zero activity, $m = 0$, are states of minimal energy, among which the P patterns need to be discriminated. To this end, we choose the bare kinetic parameters such that transitions that increase the overlap with the patterns are accelerated. In particular, we set

$$\omega(\boldsymbol{\sigma}, \boldsymbol{\sigma}') = \begin{cases} 1, & \text{if } h_i \geq 0, \\ \exp(-Q), & \text{if } h_i < 0, \end{cases} \quad (4)$$

where $Q \geq 0$ is a discrimination barrier in units of β^{-1} , and $h_i(\boldsymbol{\sigma}) = \sum_{j \neq i} J_{ij} \sigma_j$ is the effective field acting on unit i , which is the unit that changes between $\boldsymbol{\sigma}$ and $\boldsymbol{\sigma}'$. Since $h_i(\boldsymbol{\sigma})$ does not depend on σ_i , it follows that ω is symmetric with respect to the exchange $\boldsymbol{\sigma} \leftrightarrow \boldsymbol{\sigma}'$.

The choice of the expressions for \mathcal{H} and ω made above can be justified as follows. Suppose that the system is initially set in a state such that a random fraction m_1 of units respects pattern $\mu = 1$, while the rest is inactive ($\sigma_i = -1$), and so $m = m_1 - 1 < 0$, see SI. In this case, the energy function of Eq. (3) tends to increase the activity toward $m = 0$ by activating the inactive units indiscriminately. However, as per Eq. (4), the units with a positive local field will tend to activate first. Using Eq. (2), we find that $h_i = \sum_{\mu} \xi_i^\mu m_\mu - \sigma_i P / N$, which, given $m_1 \gg P / N$, approximates to $h_i \approx \xi_i^1 m_1$. This implies that the first units to activate will be the ones for which $\xi_i^1 = +1$. Therefore, we expect that the combination of these two effects results in activating the inactive units that are active in pattern 1, see Fig. 1D. The correction of these “ -1 errors” ($\sigma_i = -1$ while $\xi_i^1 = +1$) will lead to the simultaneous increase of m_1 and m over time t . In other words, we expect the present kinetic encoding model to perform pattern retrieval, provided that the non-cue part of the network is inactivated. In the following, we support this argument through extensive numerical simulations and analytical calculations.

Retrieval of a single pattern. As a starting point, we suppose that the couplings encode a single pattern ($P = 1$). In this case, the network can be described by two quantities, namely the fractions of -1 errors and $+1$ errors, the latter referring to units with $\sigma_i = +1$ while $\xi_i^1 = -1$, see SI. Based on the conceptual energy landscapes of Figs. 1B and D, we expect that retrieval of the pattern requires large values of the energetic drive K and of the discrimination barrier Q . In fact, Fig. 2 shows

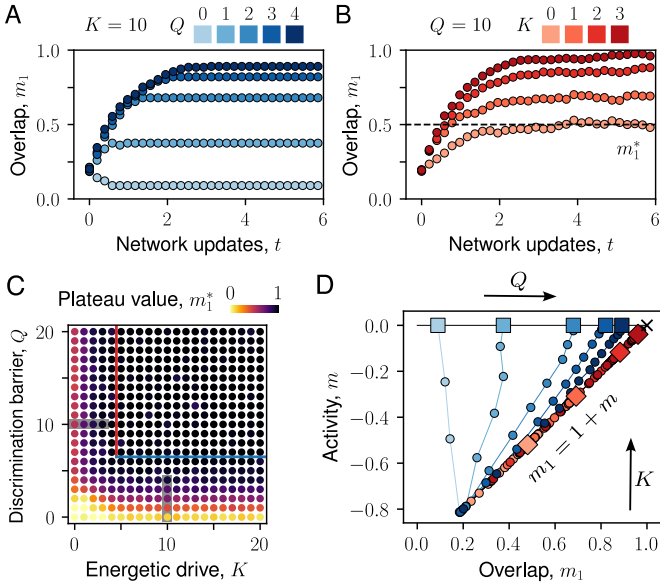


FIG. 2. *Successful retrieval of a single pattern.* **A.** Stochastic trajectories for $P = 1$ and $N = 2^{10}$, starting from a random state with $m_1 = 0.2$ and $m = -0.8$, see SI for simulation details. At a fixed value $K = 10$, m_1 evolves toward a plateau whose value m_1^* increases with Q . **B.** At $Q = 10$, the plateau value increases with K . The small fluctuations around the plateau value disappear with increasing K . **C.** Phase diagram of pattern retrieval. The plateau value m_1^* corresponds to a 1% error for Q and K above the analytical estimates ≈ 6.9 and 4.6 respectively (blue and red lines) [SI]. The grey regions refer to the time trajectories shown in A-B. **D.** The blue trajectories from **A** have plateau values $m_1^* \approx 0$ (larger squares), while for the red trajectories from **B**, $m_1^* \approx 1 + m_1^*$.

that this is the case, with m_1 reaching values close to 1 for high K and Q . In contrast, if Q is low (Fig. 2A), the descent in the energy function \mathcal{H} (Eq. (3)) is unbiased, and thus the system gets trapped in an arbitrary state. On the other hand, if K is low (Fig. 2B), the system will diffuse in a flat energy landscape, and the overlap saturates at an intermediate value. Therefore, both high K and high Q are necessary for pattern retrieval.

In the SI, we analytically determine the conditions under which the system can retrieve a pattern from a cue. We find that for K and Q above certain thresholds K_{\min} and Q_{\min} , the system successfully reaches the pattern state. Specifically, considering success as achieving less than 1% error in the average overlap ($m_1 = 0.99$), in the thermodynamic limit $N \rightarrow \infty$, these thresholds are respectively given by $K_{\min} \approx 4.6$ and $Q_{\min} \approx 6.9$, see Fig. 2C.

To gain further insight into the retrieval of this model, we analyze trajectories of the overlap m_1 and activity m over time. In the limit $K, Q \rightarrow \infty$, Fig. 1D shows that m_1 and m increase simultaneously, such that $m_1(t) - m(t)$ is constant over time. Figure 2D displays examples of such dynamic trajectories, which, for increasing K and Q , approach the predicted pathway

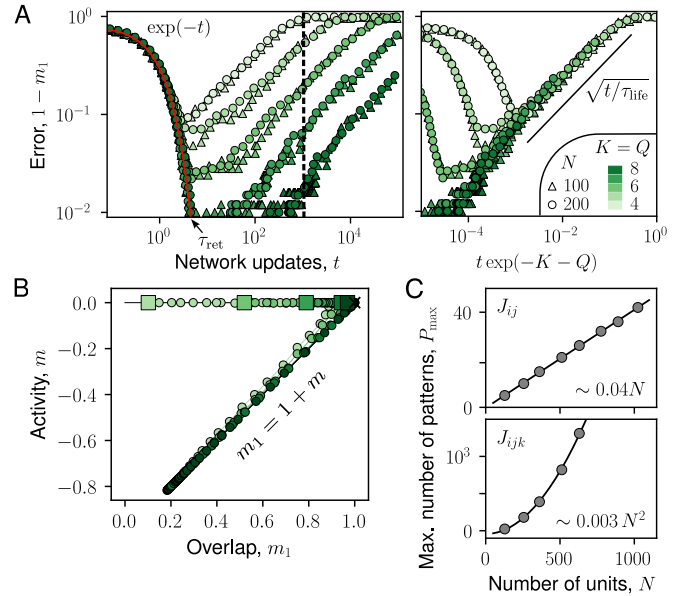


FIG. 3. *Large kinetic stability and high encoding capacity.* **A.** The system eventually escapes the kinetic trap ($m_1 = 1$) toward states with lower values of m_1 . The retrieval dynamics follows the exponential prediction (red line). The escape dynamics rescaled horizontally by the lifetime, t/τ_{life} , is similar for different values of K, Q, N with a slope of $\frac{1}{2}$ in log-log (black line). Additionally, the minimum error decreases with increasing values of K and Q . Here, $P = 1$. **B.** The trajectories in log time show that the eventual slow decrease of m_1 occurs near the $m = 0$ line. The values at time $t = 10^3$ (dashed line in **A**) are shown as larger squares. **C.** The plateau value of the overlap with the cued pattern, m_1^* , decreases with increasing number of patterns, P . For pair couplings, the encoding capacity P_{\max} at which $m_1^* = 0.95$ scales with N . Whereas for three-body couplings, P_{\max} scales with N^2 .

to the pattern, $m_1(t) = 1 + m(t)$. We note that, as anticipated before, to reach the pattern ($m_1 = 1$ and $m = 0$), the initial state must not contain any +1 errors since they cannot be corrected, *i.e.*, $m(0) = m_1(0) - 1$, see SI.

Kinetic stability of the pattern. Our model encodes patterns kinetically in the form of kinetic traps, from which the system will eventually escape. We quantify the kinetic stability of patterns by the ratio of their lifetime to their retrieval time. We obtain the retrieval time τ_{ret} , measured in number of network updates, by approximating the dynamics as follows. For $K, Q \rightarrow \infty$, the limiting process during retrieval consists in finding the -1 errors to correct, so that the average error fraction $1 - m_1$ decreases at a rate equal to its value [SI]. Therefore, in the thermodynamic limit $N \rightarrow \infty$, the average error fraction decreases as $\exp(-t)$. We conclude that the retrieval time, τ_{ret} , is independent of K, Q and N . Defining τ_{ret} as the time at which m_1 reaches the value 0.99 starting from $m_1(0) = 0.2$, we obtain $\tau_{\text{ret}} \approx 4.4$, in agreement with the simulation data in Fig. 3A.

After retrieval of the pattern ($m_1 \approx 1$ and $m \approx 0$), the system remains near the energy minima $m = 0$, but slowly drifts away from the pattern state. This can be seen in the eventual decrease of m_1 in Fig. 3A-B. The reason behind this drift is that states with $m = 0$ but lower values of m_1 are more numerous and thus entropically favored. The slow decrease in m_1 occurs through double errors, *i.e.*, deactivation of a unit and subsequent activation of another, to keep the overall network activity close to 0. These double errors occur with a rate $\sim \exp(-K)\exp(-Q)$, as sketched in Fig. 1D.

This escape dynamics is more complex than the retrieval dynamics, but we can estimate the lifetime of the patterns as the time to make a fraction of N double errors, which gives a number of network updates $\tau_{\text{life}} \sim \exp(K+Q)$, see SI. Therefore, the ratio of lifetime to retrieval time is given by

$$\tau_{\text{life}}/\tau_{\text{ret}} \sim \exp(K+Q), \quad (5)$$

and so large values of K and Q result in long-lived patterns relative to their retrieval time, as shown in Fig. 3A. We observe that the eventual error increases approximately as $1-m_1 \sim \sqrt{t}/\tau_{\text{life}}$, a behavior for which we have not yet been able to provide an explanation. (A diffusive behavior would yield a square-root dependence not for the average error but for the fluctuations around that average.) To conclude, we have shown that the kinetic encoding approach in Eqs. (3-4) allows for the fast retrieval of a single pattern for strong discrimination and large driving.

Encoding capacity. We now turn to the case where the couplings encode multiple patterns ($P > 1$). In this scenario, errors arise from crosstalk between patterns, which become more and more prevalent as P increases. For the same large positive values of K and Q that lead to retrieval for $P = 1$, if the number of stored patterns is above a certain maximal value, $P > P_{\text{max}}$, retrieval becomes impossible due to crosstalk. We find that the encoding capacity P_{max} scales linearly with the system size N as in the classical case of energetic encoding [2], see Fig. 3C. Indeed, our kinetic encoding is based on the same quantity h_i and is therefore subject to the same crosstalk issues as the energetic encoding [SI].

To probe the performance of kinetic encoding further, we now suppose that the units interact by three-body couplings $J_{ijk} = \sum_{\mu} \xi_i^{\mu} \xi_j^{\mu} \xi_k^{\mu} / N^2$ instead of the pair couplings of Eq. (2). The local field in Eq. (4) is now given by $h_i(\boldsymbol{\sigma}) = \sum_{j,k \neq i} J_{ijk} \sigma_j \sigma_k$, which leads to an encoding capacity $P_{\text{max}} \sim N^2$, in agreement with the predictions from energetic encoding in modern Hopfield networks [26–28].

Ageing relaxation. So far, we have shown that the key differences between the kinetic and energetic Hopfield networks lie in the dynamics, not the capacity. In order to gain deeper insight into the dynamics of kinetic

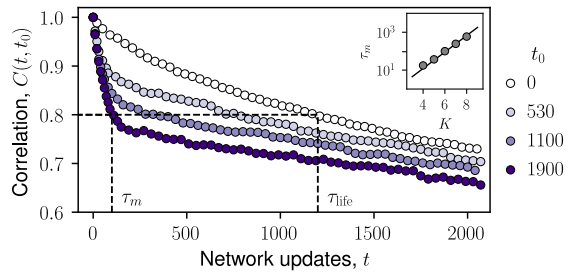


FIG. 4. *Temporal correlations are not time-translation invariant.* Beginning from the pattern state at $t = 0$, the correlation between states at times t_0 and $t + t_0$ depends on the waiting time t_0 . For $t_0 \gtrsim \tau_{\text{life}}$, $C(t, t_0)$ abruptly drops for $t \sim \tau_m$, whereas $C(t, 0)$ only significantly decreases on timescale $\tau_{\text{life}} \gg \tau_m$. Here, $N = 100$, $P = 1$, $m_1(0) = 1$ and $K = Q = 6$ such that the lifetime at which $m_1 = 0.8$ is $\tau_{\text{life}} \approx 1200$, while $C(\tau_m, 1900) = 0.8$ for $\tau_m \approx 100$. *Inset:* Timescale τ_m increases exponentially with the energetic drive, K .

encoding, we now study time correlations. We thus consider a network with pair couplings that encode a single pattern. We set the network in the pattern state, such that $\boldsymbol{\sigma}(t = 0) = (\xi_1^1, \dots, \xi_N^1)$, and investigate the escape from the pattern. We characterize this escape via the correlation between states at times t_0 and $t + t_0$ defined as:

$$C(t, t_0) = \frac{1}{N} \sum_i \sigma_i(t + t_0) \sigma_i(t_0), \quad (6)$$

averaged over the thermal noise and the patterns given by. By comparing $C(t, 0) = m_1(t)$ to the correlation function $C(t, t_0)$ for different waiting times, t_0 , we see in Fig. 4B that the curves fail to overlap. This absence of time-translation invariance is typical of glassy systems with large timescale separation [24, 25]. Importantly, unlike typical ageing glasses whose relaxation becomes slower as the waiting time t_0 increases [30], here the relaxation becomes faster as t_0 increases. This arises from an initial drop of the correlation for $t_0 \gtrsim \tau_{\text{life}}$ and $t \sim \tau_m$, the timescale over which errors move between units; see SI. This additional timescale, which scales as $\tau_m \sim \exp(K)$ (see inset), lies between the retrieval time and the pattern lifetime, and adds another level of complexity to the description of the system.

Discussion. In classical neural network models of content-associative memory, patterns are stored as distinct energy minima. Our novel kinetic encoding approach instead sculpts the pathways toward the pattern states, thereby enabling the reliable discrimination of pattern states among a sea of erroneous energy minima. We have shown using simulation and theory that the network can retrieve many kinetically encoded pattern states transiently, yet quickly. Notably, we found that the lifetime of encoded patterns can be several orders of magnitude longer than their retrieval time. The

encoding capacity moreover attains similar scaling than for classical Hopfield networks [2, 28]. Our model however presents an important limitation as retrieval is only possible if the non-cue part of the pattern is inactive. We expect that this limitation, less severe for sparse patterns, can be circumvented by the appropriate usage of neural activation thresholds.

This work builds on a previous study of kinetic encoding in polymerizing strings, where we similarly observed the rapid retrieval of multiple heteromeric target structures from the same components [20]. Therefore, we expect that the same design principles outlined here can be applied to other memory retrieval systems, in

particular physical systems where the detailed balance condition plays a central role [12, 31, 32]. Beyond the retrieval of static (or evolving [33]) patterns, kinetic encoding also holds potential for applications in the retrieval of memory sequences [34–36] – an area of research that has become particularly active in the context of learning within physical systems [37–40].

Acknowledgments. This work was partly supported by a laCaixa Foundation grant (LCF/BQ/PI21/11830032) and core funding from the Gulbenkian Foundation.

-
- [1] W. Gerstner, W. M. Kistler, R. Naud, and L. Paninski, *Neuronal Dynamics: From Single Neurons to Networks and Models of Cognition* (Cambridge University Press, 2014).
- [2] J. Hertz, A. Krogh, and R. G. Palmer, *Introduction to the Theory of Neural Computation*, Santa Fe Institute Series (CRC Press, 1991).
- [3] H. Ramsauer, B. Schäffl, J. Lehner, P. Seidl, M. Widrich, L. Gruber, M. Holzleitner, T. Adler, D. Kreil, M. K. Kopp, G. Klambauer, J. Brandstetter, and S. Hochreiter, in *International Conference on Learning Representations* (2021).
- [4] J. J. Hopfield, *Proc. Natl. Acad. Sci. U.S.A.* **79**, 2554 (1982).
- [5] D. J. Amit, H. Gutfreund, and H. Sompolinsky, *Phys. Rev. Lett.* **55**, 1530 (1985).
- [6] D. Krotov, *Nature Reviews Physics* **5**, 366 (2023).
- [7] Y. Liang, D. Krotov, and M. J. Zaki, *Frontiers in Big Data* **5** (2022), 10.3389/fdata.2022.1044709.
- [8] P. Mehta, M. Bukov, C.-H. Wang, A. G. Day, C. Richardson, C. K. Fisher, and D. J. Schwab, *Physics Reports* **810**, 1 (2019).
- [9] D. Krotov and J. J. Hopfield, in *International Conference on Learning Representations* (2021).
- [10] W. F. Podlaski and C. K. Machens, “Storing overlapping associative memories on latent manifolds in low-rank spiking networks,” (2024), arXiv:2411.17485 [q-bio.NC].
- [11] M. I. Rabinovich, P. Varona, A. I. Selverston, and H. D. I. Abarbanel, *Rev. Mod. Phys.* **78**, 1213 (2006).
- [12] R. B. Teixeira, G. Carugno, I. Neri, and P. Sartori, *Proc. Natl. Acad. Sci. U.S.A.* **121**, e2320504121 (2024).
- [13] C. G. Evans, J. O’Brien, E. Winfree, and A. Murugan, *Nature* **625**, 500 (2024).
- [14] A. Murugan, Z. Zeravcic, M. P. Brenner, and S. Leibler, *Proc. Natl. Acad. Sci. U.S.A.* **112**, 54 (2015).
- [15] P. Sartori and S. Leibler, *Proc. Natl. Acad. Sci. U.S.A.* **117**, 114 (2020).
- [16] O. Karin, *bioRxiv* (2024), 10.1101/2024.02.03.578744.
- [17] C. H. Bennett, *Biosystems* **11**, 85 (1979).
- [18] P. Sartori and S. Pigolotti, *Phys. Rev. Lett.* **110**, 188101 (2013).
- [19] Y.-C. Tsai and K. A. Johnson, *Biochemistry* **45**, 9675 (2006), pMID: 16893169.
- [20] F. Benoist and P. Sartori, *Phys. Rev. Lett.* **134**, 038402 (2025).
- [21] J. J. Hopfield, *Proc. Natl. Acad. Sci. U.S.A.* **71**, 4135 (1974).
- [22] R. Ravasio, K. Husain, C. G. Evans, R. Phillips, M. Ribezzi, J. W. Szostak, and A. Murugan, “A minimal scenario for the origin of non-equilibrium order,” (2024), arXiv:2405.10911 [q-bio.PE].
- [23] B. Lefebvre and C. Maes, *J. Stat. Phys.* **190**, 90 (2023).
- [24] J.-P. Bouchaud, L. F. Cugliandolo, J. Kurchan, and M. Mézard, “Out of equilibrium dynamics in spin-glasses and other glassy systems,” in *Spin Glasses and Random Fields* (1997) pp. 161–223.
- [25] J. Bouchaud, *Journal de Physique I* **2**, 1705 (1992).
- [26] D. Krotov and J. J. Hopfield, in *Advances in Neural Information Processing Systems*, Vol. 29, edited by D. Lee, M. Sugiyama, U. Luxburg, I. Guyon, and R. Garnett (Curran Associates, Inc., 2016).
- [27] C. M. Newman, *Neural Networks* **1**, 223 (1988).
- [28] M. Demircigil, J. Heusel, M. Löwe, S. Uppgang, and F. Vermet, *Journal of Statistical Physics* **168**, 288 (2017).
- [29] I. Kanter and H. Sompolinsky, *Phys. Rev. A* **35**, 380 (1987).
- [30] L. Berthier and J.-P. Bouchaud, *Phys. Rev. B* **66**, 054404 (2002).
- [31] K. E. Dunn, F. Dannenberg, T. E. Ouldrige, M. Kwiatkowska, A. J. Turberfield, and J. Bath, *Nature* **525**, 82 (2015).
- [32] L. Yan, R. Ravasio, C. Brito, and M. Wyart, *Proc. Natl. Acad. Sci. U.S.A.* **114**, 2526 (2017).
- [33] O. H. Schnaack, L. Peliti, and A. Nourmohammad, *Phys. Rev. X* **12**, 021063 (2022).
- [34] H. Sompolinsky and I. Kanter, *Phys. Rev. Lett.* **57**, 2861 (1986).
- [35] P. Seliger, L. S. Tsimring, and M. I. Rabinovich, *Phys. Rev. E* **67**, 011905 (2003).
- [36] L. Herron, P. Sartori, and B. Xue, *PRX Life* **1**, 023012 (2023).
- [37] M. Stern, M. B. Pinson, and A. Murugan, *Phys. Rev. X* **10**, 031044 (2020).
- [38] N. C. Keim, J. D. Paulsen, Z. Zeravcic, S. Sastry, and S. R. Nagel, *Rev. Mod. Phys.* **91**, 035002 (2019).
- [39] R. Mandal, R. Huang, M. Fruchart, P. G. Moerman, S. Vaikuntanathan, A. Murugan, and V. Vitelli, “Learning dynamical behaviors in physical systems,” (2024), arXiv:2406.07856 [cond-mat.soft].

Supporting information for “Content-Addressable Memory with a Content-Free Energy Function”

I. ESTIMATION OF ENCODING CAPACITY

The encoding capacity for energetic and kinetic encoding can be estimated via a simple argument based on the stability of pattern states as follows [2].

Energetic encoding. We focus on the case where the transition rate from state $\boldsymbol{\sigma} = (\sigma_1, \dots, \sigma_i, \dots, \sigma_N)$ to $\boldsymbol{\sigma}' = (\sigma_1, \dots, -\sigma_i, \dots, \sigma_N)$ is given by Eq. (1) with $\Delta E(\boldsymbol{\sigma}, \boldsymbol{\sigma}') = 2h_i\sigma_i$ and $\omega(\boldsymbol{\sigma}, \boldsymbol{\sigma}') = 1$. At zero temperature, *i.e.* $\beta \rightarrow \infty$, the dynamics reduces to a straightforward update rule for the activity σ_i of each unit i :

$$\sigma_i = \text{sgn } h_i = \text{sgn} \left(\sum_{j \neq i} J_{ij} \sigma_j \right), \quad (\text{S1})$$

where $J_{ij} = \frac{1}{N} \sum_{\mu} \xi_i^{\mu} \xi_j^{\mu}$ [Eq. (2)]. The stability of pattern $\mu = 1$ depends on its crosstalk with the remaining patterns, which we evaluate via $C_i^1 = \frac{1}{N} \sum_{j \neq i} \sum_{\mu > 1} \xi_i^{\mu} \xi_j^{\mu} \xi_j^1 \xi_i^1$. In the limit $N, P \rightarrow \infty$ and for $\boldsymbol{\sigma} = (\xi_1^1, \dots, \xi_N^1)$, we decompose the local field as

$$h_i = \frac{N-1}{N} \xi_i^1 + \frac{1}{N} \sum_{j \neq i} \sum_{\mu > 1} \xi_i^{\mu} \xi_j^{\mu} \xi_j^1 \approx \xi_i^1 (1 + C_i^1). \quad (\text{S2})$$

Therefore, the update rule $\sigma_i \approx \xi_i^1 \text{sgn}(1 + C_i^1)$ leads to the stability of pattern 1 unless the crosstalk term C_i^1 is smaller than -1 . Given random patterns with equal probabilities of $\xi_i^{\mu} = \pm 1$, C_i^1 is $\frac{1}{N}$ times the sum of NP random variables with values ± 1 . It thus has zero mean and variance $\alpha = P/N$, which gives the rudimentary zero-temperature stability condition $\alpha < 1$, *i.e.*,

$$P < N. \quad (\text{S3})$$

More precise calculations give stability thresholds on the order of $\alpha_c \approx 0.14$, *i.e.* $P_c \approx 0.14N$ [2, 5]. However, for such values of α , the pattern states correspond only to local minima, which are metastable. They instead become global minima for values of α smaller than $\alpha_{\max} \approx 0.05$, *i.e.* $P_{\max} \approx 0.05N$. Thus, pair interactions can encode a number of patterns proportional to the system size.

Moreover, the inclusion of higher-order couplings has been shown to drastically increase encoding capacity [26–28]. For instance, three-body couplings that lead to pattern retrieval are given by $J_{ijk} = \sum_{\mu} \xi_i^{\mu} \xi_j^{\mu} \xi_k^{\mu} / N^2$, with a local field $h_i(\boldsymbol{\sigma}) = \sum_{j, k \neq i} J_{ijk} \sigma_j \sigma_k$. Following the same argument as above, we decompose the local field as $h_i \approx \xi_i^1 (1 + D_i^1)$, with a crosstalk term $D_i^1 = \frac{1}{N^2} \sum_{j, k \neq i} \sum_{\mu > 1} \xi_i^{\mu} \xi_j^{\mu} \xi_k^{\mu} \xi_j^1 \xi_k^1 \xi_i^1$. This results in the stability condition

$$P < N^2, \quad (\text{S4})$$

which can be made more precise according to similar arguments as above.

Kinetic encoding. For kinetic encoding, the transition rate $k(\boldsymbol{\sigma} \rightarrow \boldsymbol{\sigma}')$ from Eq. (1) has parameters

$$\beta \Delta E(\boldsymbol{\sigma}, \boldsymbol{\sigma}') = \begin{cases} -K \sigma_i \text{sgn } m, & \text{if } m \neq 0, \\ K, & \text{if } m = 0, \end{cases} \quad (\text{S5})$$

and $\omega(\boldsymbol{\sigma}, \boldsymbol{\sigma}')$ as in Eq. (4). The zero-temperature update rule for $m(\boldsymbol{\sigma}) < 0$ thus amounts to

$$\sigma_i = \begin{cases} \text{sgn } h_i, & \text{if } \sigma_i = -1, \\ \sigma_i, & \text{if } \sigma_i = +1. \end{cases} \quad (\text{S6})$$

Therefore, inactive units are updated based on their field h_i , until the overall activity vanishes, *i.e.* $m = 0$. This fundamentally distinguishes our kinetic encoding model from the case of energetic encoding described above, in which both active and inactive units are updated at zero temperature [Eq. (S1)]. As emphasized in the text, since the stability criterion for energetic depends only on the field h_i acting on unit i , it applies also to kinetic encoding.

II. THEORY FOR PATTERN RETRIEVAL AND ESCAPE IN KINETIC ENCODING

We hereby set out to properly describe the states and transitions of a network with one kinetically encoded pattern, *i.e.* $P = 1$. We then write dynamical equations that we finally solve in the regime of large values of K, Q and N . This yields the thresholds K_{\min} and Q_{\min} for retrieval, the retrieval time τ_{ret} and lifetime τ_{life} , and the limit trajectory of m_1 and m for $K, Q \rightarrow \infty$.

Detailed description of the system. For $P = 1$, as shown in Fig. 1D, the units fall into four categories depending on their activity $\sigma_i = \pm 1$ and target activity $\xi_i^1 = \pm 1$. We annotate them using green plus and minus signs if they respect the (green) pattern, and with black symbols otherwise. The corresponding fractions of units written f_+, f_-, f_+ and f_- satisfy the relationships $f_+ + f_- = f_- + f_+ = \frac{1}{2}$, since the target activities ± 1 are equiprobable. We thus further describe any state of the network, $\boldsymbol{\sigma} = (\sigma_1, \dots, \sigma_N)$, solely in terms of the error fractions f_- and f_+ , from which the activity and overlap result as

$$m = 2(f_+ - f_-) \quad \text{and} \quad m_1 = 1 - 2(f_+ + f_-). \quad (\text{S7})$$

In particular, if $m = m_1 - 1$, then $f_+ = 0$, such that there are only -1 errors and no $+1$ errors.

With this notation, we can rewrite the Glauber transition rates $k(\boldsymbol{\sigma} \rightarrow \boldsymbol{\sigma}')$ from Eqs. (1-4) into four expressions depending on the type of event: correction/creation of a -1 error, $k_{-\rightarrow+}, k_{+\rightarrow-}$, and correction/creation of a $+1$ error, $k_{+\rightarrow-}, k_{-\rightarrow+}$. We introduce $\gamma = (1 + e^{-K})^{-1}$ and consider significant overlap values, $m_1 \gg 1/N$, such that the local field can be approximated as $h_i = \xi_i^1 m_1 - \sigma_i/N \approx \xi_i^1 m_1$. The rates then depend of the activity m as

$$\begin{cases} k_{-\rightarrow+} = \gamma, & k_{+\rightarrow-} = \gamma e^{-K}, & k_{-\rightarrow+} = \gamma e^{-Q}, & k_{+\rightarrow-} = \gamma e^{-K-Q}, & \text{for } m < 0, \\ k_{-\rightarrow+} = \gamma e^{-K}, & k_{+\rightarrow-} = \gamma e^{-K}, & k_{-\rightarrow+} = \gamma e^{-K-Q}, & k_{+\rightarrow-} = \gamma e^{-K-Q}, & \text{for } m = 0, \\ k_{-\rightarrow+} = \gamma e^{-K}, & k_{+\rightarrow-} = \gamma, & k_{-\rightarrow+} = \gamma e^{-K-Q}, & k_{+\rightarrow-} = \gamma e^{-Q}, & \text{for } m > 0. \end{cases} \quad (\text{S8})$$

Given the interchangeability of units with the same activity and target activity, these transition rates need to be multiplied by entropic factors to properly describe the dynamics of the error fractions. This can be visualized in the transition diagram sketched in Fig. S1.

Dynamical equations for the error fractions. Now that the system is properly defined, we can investigate its dynamical evolution. As the network is updated spin by spin, the time t measured in number of network updates increases by steps of size $\delta t = 1/N$. The error fractions evolve stochastically between time intervals with steps of size $\delta f = 1/N$. As long as $m = 2(f_+ - f_-) < 0$, given the rates in Eq. (S8), f_{\pm} follow two non-coupled random walks with drift, $f_{\pm}(t + \delta t) - f_{\pm}(t) = \eta_{\pm}(t)\delta f$, where the noises, η_{\pm} , are given by

$$\eta_+ = \begin{cases} 1, & \text{with prob. } \gamma e^{-Q}(\frac{1}{2} - f_+), \\ -1, & \text{with prob. } \gamma e^{-K-Q}f_+, \end{cases} \quad \text{and} \quad \eta_- = \begin{cases} 1, & \text{with prob. } \gamma e^{-K}(\frac{1}{2} - f_-), \\ -1, & \text{with prob. } \gamma f_-. \end{cases} \quad (\text{S9})$$

In the thermodynamic limit, $N \gg 1$, more analytically tractable, the averages of f_{\pm} over many realizations (which we also denote by f_{\pm}) will thus satisfy two simple linear differential equations written

$$\frac{df_+}{dt} = \gamma e^{-Q} \left[\left(\frac{1}{2} - f_+ \right) - e^{-K} f_+ \right], \quad \text{and} \quad \frac{df_-}{dt} = \gamma \left[e^{-K} \left(\frac{1}{2} - f_- \right) - f_- \right]. \quad (\text{S10})$$

We moreover consider the regime of large energetic drive and discrimination barrier, $K, Q \rightarrow \infty$, which we expect to yield fast and accurate retrieval of the pattern. In this regime, as $\gamma \rightarrow 1$ and $\exp(-Q) \rightarrow 0$, there is a large separation of timescales between the temporal variations of the error fractions f_- and f_+ . Thus, at first, f_+ remains approximately constant while f_- decreases toward the value $\frac{1}{2}\gamma e^{-K} \rightarrow 0$ at which $\frac{d}{dt}f_- = 0$. However, once f_- reaches f_+ and $m = 0$, the distribution of the noises, η_{\pm} , according to Eq. (S8) now becomes

$$\eta_+ = \begin{cases} 1, & \text{with prob. } \gamma e^{-K-Q}(\frac{1}{2} - f_+), \\ -1, & \text{with prob. } \gamma e^{-K-Q}f_+, \end{cases} \quad \text{and} \quad \eta_- = \begin{cases} 1, & \text{with prob. } \gamma e^{-K}(\frac{1}{2} - f_-), \\ -1, & \text{with prob. } \gamma e^{-K}f_-. \end{cases} \quad (\text{S11})$$

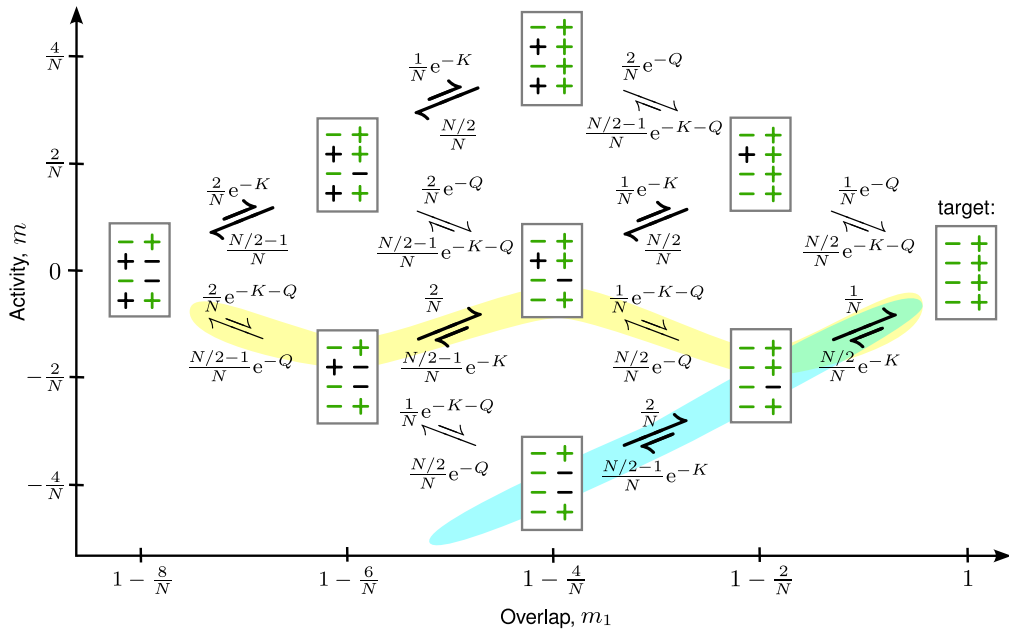


FIG. S1. *Kinetic diagram of the retrieval and escape dynamics.* Here, the transition rates are taken from Eq. (S8) in the limit $K, Q \rightarrow \infty$ where $\gamma \rightarrow 1$, with entropic factors taking into account the interchangeability of units that give the same values of m and m_1 . The limit trajectory for $K, Q \rightarrow \infty$ roughly consists of following first the blue path and then the yellow path. On the blue retrieval path, the overlap $m_1 = 1 - 2f_-$ increases via \nearrow transitions with rate given by f_- , the fraction of -1 errors (black minus signs). The yellow escape path consists of double errors (a black $+$ and a black $-$) with rates $\sim \exp(-K - Q)$. The -1 error in the state ($m_1 = 1 - \frac{4}{N}, m = 0$) can move around on timescale $\tau_m \sim \exp(K)$, by passing through the states ($m_1 = 1 - \frac{6}{N}, m = -\frac{2}{N}$) or ($m_1 = 1 - \frac{2}{N}, m = \frac{2}{N}$).

Since $m = 0$ is a stable state of the potential $K|m|$, the fast-varying function f_- will tend to stay close to f_+ , while the slow-varying function f_+ dictates the complex long-time dynamics, with a timescale $\sim \exp(K + Q)$.

Solutions of the dynamical equations. We now set out to solve the set of dynamical equations derived above for large values of K, Q and N . From an initial state with $f_-(0) > f_+(0)$, the average fraction of $+1$ errors, f_+ , will at first remain close to its initial value, while the average fraction of -1 errors, f_- , decreases toward its kinetically stable value $f_-^* \approx \max\{\frac{1}{2}\gamma e^{-K}, f_+(0)\}$. Both will then monotonically reach their steady-state values $f_+^{\text{ss}} = f_-^{\text{ss}} = \frac{1}{4}$. On average, the activity m and overlap m_1 , defined in Eq. (S7), will thus at first both increase from their initial values to reach kinetically stable values m^* and m_1^* . In the limit $K, Q \rightarrow \infty$ and $N \gg 1$ and for $f_+(0) = 0$, these read

$$m^* \approx -\frac{1}{1 + \exp K} \quad \text{and} \quad m_1^* \approx 1 + m^*, \quad (\text{S12})$$

in agreement with the simulated data shown in Fig. S2A. The minimum value of K needed to obtain only 1% error ($m_1 = 0.99$) is thus $K_{\text{min}} \approx 4.6$. During retrieval, $m_1 = 1 - 2f_-$, where Eq. (S10) prescribes that $f_-(t) \approx f_-(0) \exp(-t)$. The retrieval time to reach $m_1 = 0.99$ from $m_1(0) = 0.2$ thus reads $\tau_{\text{ret}} \approx 4.4$, in agreement with the data in Fig. S3A. Moreover, the activity and overlap are related as

$$m_1(t) \approx 1 + m(t) \quad (\text{S13})$$

during the whole retrieval phase, see the blue path in Fig. S1. While the steady-state activity is already attained, $m^{\text{ss}} = m^*$, the overlap m_1 will then monotonically reach its steady-state value $m_1^{\text{ss}} = 0$. The escape of m_1 from the kinetic trap (yellow path in Fig. S1) occurs on a timescale corresponding to the pattern lifetime, which we estimate as the rate to make $\sim N$ double errors, $\tau_{\text{life}} \sim \exp(K + Q)$, in agreement with the data in Fig. S3B. This yields Eq. (5) in the main text.

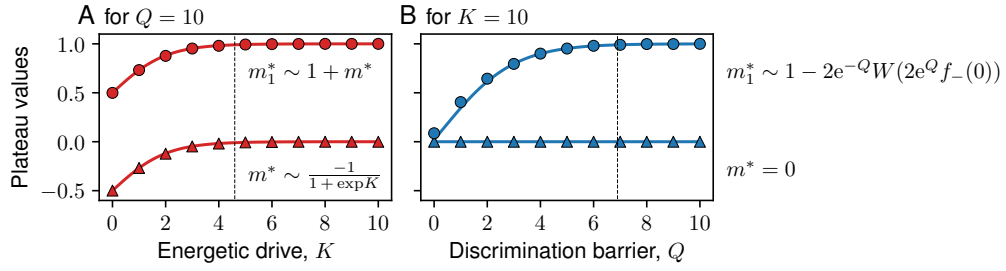


FIG. S2. *Kinetically stable values.* This shows the dependence of the plateau values from trajectories of the type in Fig. 2A-B. **A.** For large Q , the overlap m_1^* and activity m^* satisfy Eq. (S12). The dashed line denotes the analytical estimate for 1% error, $K_{\min} \approx 4.6$. **B.** For large K , the overlap m_1^* satisfies Eq. (S15), while $m^* = 0$. The dashed line denotes the analytical estimate for 1% error, $Q_{\min} \approx 6.9$. Here, as in Fig. 2, $m_1(0) = 0.2$ and $m(0) = -0.8$, such that $f_-(0) = 0.4$ and $f_+(0) = 0$.

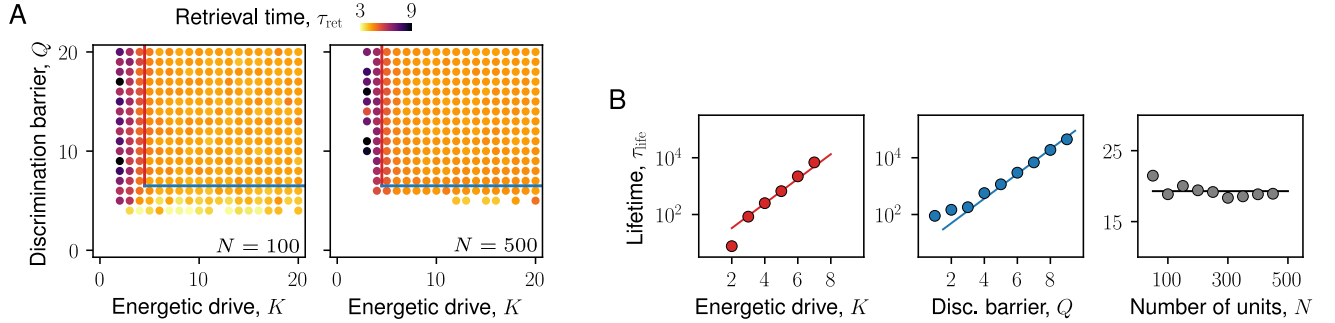


FIG. S3. *Characteristic timescales verify predictions.* **A.** The retrieval time, estimated in retrieval trajectories as the time at which $m_1 = 0.99$, satisfies the analytical estimate, $\tau_{\text{ret}} \approx 4.4$, within the retrieval region (inside the blue and red lines). Here, $P = 1$, $m_1(0) = 0.2$ and $m(0) = 0.8$. **B.** The lifetime, estimated in escape trajectories as the time at which $m_1 = 0.8$, satisfies the analytical estimate, $\tau_{\text{life}} \sim \exp(K + Q)$. Here, $P = 1$, $m_1(0) = 1$ and $m(0) = 0$, and we vary K , Q or N while keeping the other two constant.

To obtain the dependence of m_1^* on Q and thus the threshold Q_{\min} , we consider the limit $K \rightarrow \infty$. For $f_+(0) = 0$, by solving Eq. (S10) we find that the average fractions evolve as

$$f_+(t) \approx \frac{1}{2}(1 - e^{-\exp(-Q)t}) \quad \text{and} \quad f_-(t) \approx f_-(0)e^{-t} \quad (\text{S14})$$

until they meet at a time which in the limit $Q \rightarrow \infty$ approaches $W(2e^Q f_-(0))$, where W is the Lambert function. This defines the kinetically stable state with activity $m^* = 2(f_+^* - f_-^*) = 0$ and overlap

$$m_1^* \approx 1 - 2e^{-Q}W(2e^Q f_-(0)). \quad (\text{S15})$$

This is in agreement with the data in Fig. S2B. The minimum value of Q to obtain only 1% error is thus $Q_{\min} \approx 6.9$.

Additionally, in the presence of +1 errors with $f_+(0) \gg \frac{1}{2}(1 + e^K)^{-1}$ and for $K, Q \rightarrow \infty$, we instead find

$$m^* = 0, \quad \text{and} \quad m_1^* \approx 1 - 4f_+(0) \approx m_1(0) - m(0). \quad (\text{S16})$$

Moreover, since Eq. (S10) prescribes $\frac{d}{dt}f_- \approx -f_- \gg \frac{d}{dt}f_+$, we approximate that the average fraction of -1 errors, f_- , decreases at constant f_+ . This is such that the retrieval trajectory satisfies the equation

$$m_1(t) - m(t) \approx m_1(0) - m(0), \quad (\text{S17})$$

in agreement with the data in Fig. S4. This concludes our analytical investigation of the retrieval and escape dynamics.

III. SIMULATION DETAILS

To model the network dynamics, we perform Monte Carlo simulations with the Metropolis algorithm. We choose P random patterns, we set the couplings J_{ij} based on Eq. (2), and we set the values of the N units with a random

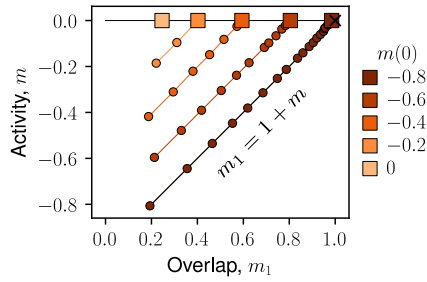


FIG. S4. *Limit trajectories from initial states with different activities.* The trajectories in the limit $K, Q \rightarrow \infty$ are linear and satisfy Eq. (S17) until the plateau with values $m^* = 0$ and $m_1^* = m_1(0) - m(0)$ (larger filled markers). Here, all trajectories have $K = Q = 6$, $N = 2^{10}$, $P = 1$ and $m_1(0) = 0.2$.

cue of pattern $\mu = 1$, such that $m_1(0) = 0.2$ and $m(0) = -0.8$. We make sure that these initial values satisfy the condition $m_1(0) = 1 + m(0)$, necessary to reach the pattern state ($m_1 = 1, m = 0$), see Fig. S4. Then, at each iteration, we randomly select a unit and change its activity with a probability equal to its Glauber transition rate [Eq. (S8)].

IV. THEORY FOR THE AGEING RELAXATION

Beyond the decrease in overlap, from $m_1(0) = 1$ to $m_1(\tau_{\text{life}}) = 0.8$, we characterize the escape from the pattern via the correlation $C(t, t_0)$ between states at times t_0 and $t + t_0$, defined in Eq. (6). Figure 4 shows a clear dependence of $C(t, t_0)$ on the waiting time t_0 , incompatible with the description of the escape based on a single timescale, *i.e.* the lifetime, $\tau_{\text{life}} \sim \exp(K + Q)$. To explain this ageing phenomenon, we introduce another timescale, $\tau_m \sim \exp(K)$, which characterizes the movement of -1 errors among the units with target activity $+1$, see Fig. S1. For large values of K and Q , we thus distinguish three regimes:

- (i) On short timescales, $t \ll \tau_m$, $C(t, 0) = m_1(t) \approx 1$ and $C(t, t_0) \approx 1$, whatever t_0 .
- (ii) On intermediate timescales, $\tau_m \lesssim t \ll \tau_{\text{life}}$, $C(t, 0) \lesssim 1$, because relatively few double errors will have occurred. In contrast, for $C(t, t_0)$ with $t_0 \gtrsim \tau_{\text{life}}$, the many errors in the state $\sigma(t_0)$ with overlap $m_1(t_0) \approx 0.8$ will tend to move around in the time window $[t_0, t + t_0]$. This will cause discrepancies with the state $\sigma(t + t_0)$, which explains the important drop in correlation.
- (iii) On longer timescales, $t \gtrsim \tau_{\text{life}}$, both $C(t, 0)$ and $C(t, t_0)$ will decrease significantly with t .

This explains the absence of time-translation invariance displayed in Fig. 4. The dependence of τ_m on the energetic drive K and on the discrimination barrier Q is validated in Fig. S5.

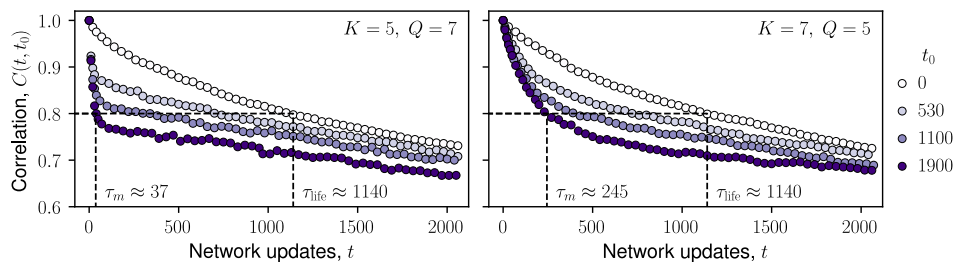


FIG. S5. *The timescale of the correlation drop can be varied independently of the lifetime.* We define τ_{life} and τ_m as the times such that $C(\tau_{\text{life}}, 0) = 0.8$ and $C(\tau_m, 1900) = 0.8$. Like so, we can increase $\tau_m \sim \exp(K)$ at constant $\tau_{\text{life}} \sim \exp(K + Q)$ by increasing K while decreasing Q . Here, $N = 100$, $P = 1$, and $m_1(0) = 1$, as in Fig. 4.